• Basic Research •

Ultrasound-targeted cationic microbubble-mediated gene transfection and inhibition of retinal neovascularization

Ming-Xing Wu, Yu Zhou, Xi-Yuan Zhou, Yan Xu

Department of Ophthalmology, Second Affiliated Hospital of Chongqing Medical University, Chongqing 400010, China

Correspondence to: Yan Xu. Department of Ophthalmology, Second Affiliated Hospital of Chongqing Medical University, 74 Linjiang Road, Yuzhong District, Chongqing 400010, China. 301336@hospital.cqmu.edu.cn

Received: 2021-04-25 Accepted: 2022-01-26

Abstract

● **AIM:** To investigate whether ultrasound-targeted cationic microbubbles (CMBs) destruction could deliver endostatin-green fluorescent protein (GFP) plasmids efficiently to the human retinal endothelial cells (HRECs) and inhibit retinal neovascularization in mice.

● **METHODS:** CMBs were prepared and the presentation of GFP reporter was confirmed by flow cytometry and laser confocal microscopy. Experiments assessing HRECs migration and vascular formation were performed to evaluate gene therapy's efficiency *in vitro*. A mouse model of oxygen-induced retinopathy was employed and the expression of Bcl-xl, Bcl-2, vascular endothelial growth factor (VEGF) and endostatin in the retina of mice were determined by Western blotting and quantitative polymerase chain reaction (qPCR). The expression of endostatin-GFP in the retina was examined by laser confocal microscopy at 5, 14, and 28d after treatment.

● **RESULTS:** The gene expression of endostatin was the highest in the group of the CMBs. Besides, the inhibition and antiangiogenesis effect of the migration and development of HRECs were improved following treatment with CMBs compared with the other groups *in vitro*. *In vivo*, retinal neovascularization was significantly inhibited and the fluorescence intensity of endostatin-GFP in the mouse retina was importantly higher in the group of CMBs than that in other groups.

● **CONCLUSION:** The research illustrates ultrasound-targeted CMBs destruction possessed distinct effect on the inhibition of the vascular formation and the development of retinal neovascularization both *in vitro* and *in vivo*.

● **KEYWORDS:** ultrasound; cationic microbubbles; human retinal vascular endothelial cells; gene transfection; retinal neovascularization

DOI:10.18240/ijo.2022.06.04

Citation: Wu MX, Zhou Y, Zhou XY, Xu Y. Ultrasound-targeted cationic microbubble-mediated gene transfection and inhibition of retinal neovascularization. *Int J Ophthalmol* 2022;15(6):876-885

INTRODUCTION

Retinal neovascularization is a type of eye disease, and its common symptom is retinal detachment which can develop into blindness. It usually appears in prematurity's retinopathy, central vein occlusion as well as diabetic retinopathy. Current treatment of retinal neovascularization relies mainly on surgery and laser photocoagulation. Although the treatments show a certain curative impact, there're limitations and side effects. Thus, the research on a brand-new efficient treatment of retinal neovascularization has become a hot point recently. Retinal neovascularization's pathogenesis is strongly related to the balance of anti-angiogenic and pro-angiogenic elements[1], so inhibit the occurrence of new blood vessels has been the core to treat the disease.

The endostatin was chosen for its strong antiangiogenic competence. It is a 20-kDa C-terminal fragment of collagen XVIII from the hemangioendothelioma, and can inhibit angiogenesis. Endostatin is capable of inhibiting tumor growth and proliferation by suppressing angiogenesis[2]. Behl and Kotwani[3] argued that endostatin could provide a novel pharmaceutical method for the retinal neovascularization's prevention. Matsumoto *et al*[4] encapsulated endostatin into microcrystals, and observed the inhibition of migration and formation of network by microcrystals in human umbilical vein endothelial cells (HUVECs), demonstrating the anti-angiogenic activities of the endostatin. Furthermore, the endostatin microcrystals affected only the angiogenesis without any significant impact on lymphangiogenesis compared with the controls[4]. Nevertheless, the number of endostatin protein needed for creating a therapeutic impact has been rather high, and it is of great expenditure. Therefore, gene therapy might be a proper approach for exploiting the endostatin's benefits in antiangiogenesis.

Gene therapy contributes to a new approach for preventing and treating various refractory diseases. However, it exhibits many shortcomings, which limits its wide application[5]. A high level of gene transfection efficiency as well as high protein expression are in urgent need for efficient gene therapy. Researchers have defined the ultrasound-targeted microbubble destruction as a noninvasive gene transfer technology which offers a novel way to implement gene therapy[6]. Ultrasound-targeted microbubbles destruction promotes DNA's cellular uptake through the sonoporation, which allows more large molecules such as DNA enter in the cells. Microbubbles serve to be cavitation nuclei which might improve ultrasound energy deposition in tissues and decrease the energy threshold that is of great necessity for sonoporation, thereby improving the delivery of intracellular gene[7-9]. Low transfection efficiency has been the major limitation for technological, therefore many researchers are exploring the approach of overcoming this problem.

Genes are carried by microbubbles *via* electrostatic adsorption. Since the surface of cells and nucleic acids are charged negatively, the microbubbles adopted are most commonly with neutral or cationic charge, thus minimizing interaction with the cellular or molecular components in plasma[10]. It has been reported that ultrasound with cationic microbubbles (CMBs) show great ability to increase gene carrying capacity as well as remarkably improve the gene transfer[11-15]. Wang *et al*[16] pointed out that mean click beetle luciferase (CBLuc) expression had been 20-fold higher in endothelial cells when using CMBs than neutral microbubbles (NMBs), and the local gene concentration had been enhanced at therapy locations on account of positively charged microbubbles' surfaces. More importantly, CMBs can partially protect bound DNA from DNase degradation. Sun *et al*[17] synthesized CMBs capable of binding 70% more plasmid DNA relative to the commercial definity microbubbles. Ultrasound-targeted CMBs destruction using CMBs enhanced the delivery of v-akt murine thymoma viral oncogene homolog to the ischemic rat myocardium, resulting in greater cardiac functional improvements in comparison with the definity microbubbles. Panje *et al*[18] reported that gene delivery to murine hindlimb skeletal muscle under the mediation of ultrasound was enhanced by CMBs *vs* NMBs. However, the enhancement effect depended on the dose of DNA and microbubbles. With lower doses of DNA or microbubbles being used, CMBs remarkably outperformed NMBs.

In our previous study[19], we've successfully prepared the CMBs, NMBs and liposomes and initially proved that ultrasound-mediated CMBs improves endostatin-green fluorescent protein (GFP) plasmids' transfection efficiency to human retinal endothelial cells (HRECs). Here we'll search the gene transfection effect by virtue of ultrasound-mediated gene delivery using CMBs *in vivo* and *in vitro*.

MATERIALS AND METHODS

Ethical Approval The experimental protocol was established following the ethical guidelines of the Helsinki Declaration and has obtained the approval from the Human Ethics Committee of Second Affiliated Hospital of Chongqing Medical University.

Cell Culture HRECs came from TongPai Biotechnology Co., LTD (Shanghai, China) and were maintained in RPMI 1640 medium (Gibco, San Jose, CA, USA) with 100 μg/mL streptomycin, 10% fetal bovine serum (v/v; Sigma, St. Louis, MO, USA) and 100 U/mL penicillin (Sigma). The number of cells for every experiment was determined by a hemocytometer.

***In vitro* Experiments** Plasmid preparation, the characterization of NMBs and CMBs, and the plasmid binding's assessment to microbubbles had been in the same process as we reported previously[19]. We purified endostatin-GFP plasmids from *Escherichia coli*, and suspended it in MTris-HCl (pH 8.5) at 1 μg/μL. The 5 μg of plasmids (5 μL) were gently blended with 5×10^8 of a CMB or NMB suspension, with the mixture undergoing a few minutes of soft incubation at 4°C for achieving adhesion. Endostatin-GFP vector served for cell transfection assisted by Lipofectamine 2000 (Invitrogen, Carlsbad, CA, USA). We gently blended 5 μg of plasmids (5 μL) with 45 μL of RPMI-1640 medium or 3 μL of liposome plus 47 μL of RPMI-1640 medium, followed by mixing them for twenty minutes at room temperature. The Ultrasonographic Image Research Institute of Chongqing Medical University (UGT 1025 type, Chongqing, China) took charge of gene transfer. The ultrasound treatment used parameters below: continuous wave, 1 MHz, 1 W/cm^2, 20% duty cycle, 1min and a 10% concentration of microbubbles. Cultured HRECs had been classified into 4 types: 1) without any treatment (control group); 2) endostatin-GFP plasmid treated by ultrasound and NMBs (NMB group); 3) endostatin-GFP plasmids treated by liposomes (liposome group); and 4) endostatin-GFP plasmids treated by ultrasound and CMBs (CMB group). Cells in the NMB group and CMB group received 24h of incubation in an Opticell prior to transfection. The Opticell had 2 parallel breathable PS film layers and experienced a special surface treatment, thus it is suited to cell growth. The training device had an equal size with a common microporous plate. Following the injection of the microbubble composite plasmid, the Opticell was inverted for ensuring that the microbubbles can fully contact with cells, thus the effect can be maximized. The compound solution underwent 6h of incubation at 37°C with 5% CO_2, and then 500 μL of fresh media that contained 10% fetal bovine serum together with 1% penicillin/streptomycin were used to replace the compound solution. The cells

underwent another 24h of culturing, followed by the analysis of the reporter endostatin-GFP expression. Every experiment had been performed in triplicate.

Cell transfection analysis Twenty-four hours after transfection, we collected all groups of HRECs for measuring the plasmid-encoded GFP gene expression. The flow cytometry (FACS-Calibur; Becton Dickinson, San Jose, CA, USA) assisted in analyzing the transfection efficiency with an excitation setting of 488 nm. We acquired no less than 10 000 cells in each measurement. CellQuest software (BD Company, New York, NY, USA) was employed for data analysis. All experiments were conducted in triplicate.

Cell cycle analysis We collected all groups of HRECs 24h or 48h after transfection. Briefly, 0.25% trypsin-EDTA was used to harvest the HRECs which was then washed 3 times with 1 mL cold phosphate buffer saline. Then, after the addition of 1 mL of pre-cooled 70% ethanol into the cell pellet, the cells received one night of fixing at 4°C. The next day, after cell collection through centrifugation, phosphate buffer saline was used for washing cells twice. At last, the cells were resuspended again in 0.5 mL of PI solution (50 mg/mL PI, 100 mg/mL RNase A and 0.2% Triton X-100), and received 30min of incubation in the dark. The flow cytometry assisted in detecting apoptosis rate. We acquired no less than 10 000 cells in each measurement. Every experiment was performed in triplicate.

Vascular formation experiments We pre-cooled a 96-well plate, Matrigel, and serum-free RPMI-1640 culture medium. Then, RPMI 1640 culture medium free of serum diluted the Matrigel in a ratio of 2:1, and each well was added with 50 μL of the diluted Matrigel, followed by 2h of incubation at 37°C. After 24h transfection, all groups of HRECs were resuspended in RPMI 1640 medium mixed with 10% fetal bovine serum, followed by 8h of incubation at 37°C in a 5% CO_2 humidified atmosphere; each well was added with about 1×10^4 cells. An inverted microscope helped to examine the resultant tubular structures. We obtained images from 5 random fields, and calculated the tubular structure number in each field *via* direct counting. Every experiment was conducted in triplicate.

Migration experiments Migration experiments were performed using a Transwell insert with an 8 μm-pore PET membrane separating the upper and lower chambers in a 24-well plate. The HRECs belonging to different groups were harvested using 0.25% trypsin followed by being plated at 1×10^4 cells/L into the upper chamber. The upper chamber was full of a total of 100 μL of RPMI-1640 medium that contained 0.1% fetal bovine serum, and the lower chamber of the Transwell was full of 500 μL of RPMI-1640 medium that contained 10% fetal bovine serum. The HRECs received 24h of incubation at 37°C, and a cotton swab was used to scrap off the nonmigrating cells on the top of the Transwell. After being removed from the 24-well plates, the Transwells underwent 30min of staining with 0.1% crystal violet at 37°C. An inverted microscope assisted in the examination. We obtained images from five random fields, as well as calculated the invasive cell number in each field *via* Image Plus software. All the treatments were performed in triplicate.

***In vivo* Animal Experiments**

Oxygen-induced retinopathy mouse model In our study, the most widely used oxygen-induced retinopathy mouse model was adopted. Renascent C57BL/6J mice came from Chongqing Medical University's Animal Experimental Center (China). C57BL/6J mouse pups and their mothers took hyperoxia (75%±2% O_2) for five days, from postnatal day 7 (P7) to postnatal day 11 (P11). Oxygen concentrations were measured with an oxygen monitor (Ceramatec Inc., China).

Sixty mice were randomly assigned to three groups: 1) endostatin-GFP plasmid with ultrasound and NMBs (NMB group); 2) endostatin-GFP plasmids with liposomes (liposome group); and 3) endostatin-GFP plasmids with ultrasound and CMBs (CMB group). Following removal from the oxygen chamber at P12, a mixture of 1 μg of plasmids and 1 μL of microbubbles or 1 μL Lipofectamine (Invitrogen) was infused into the vitreous of the right eye, and then an ultrasound probe was immediately introduced in the NMB and CMB group, with the following parameters: continuous wave, 1 MHz, 2 W/cm^2, 1min, 50% work cycle, and a 10% of microbubbles concentration, after which the mice stayed at normoxia (room air) for 5d. The left eye of each group was set as blank control group (C group).

Histology At 5d after treatment, the mice were sacrificed, with eyes being enucleated and immediately fixed with stationary liquid (10% formaldehyde, 1% trinitrophenol, 45% dehydrated alcohol, and 35% water). Subsequently, eye dehydration was performed by a graded alcohol series and dehydrated eyes were embedded in paraffin. We cut the eyeballs in 6 μm thick serial sections, and took 10 pieces in total from each eye. The hematoxylin and eosin were employed for staining. An optical microscope helped to examine the endothelial nuclei representing new vessels that extended from the retina to the vitreous. We calculated the number of endothelial nuclei in each eye, and compared the average number for each group.

Laser scanning confocal microscopy At 5, 14, and 28d after treatment, the mice were sacrificed, with their eyes being removed, soak in 4% poly formaldehyde and then fixed 6h, dehydrated, surrounding a drop package embedding agent, frozen tissue of 10-15 μm sections. Retinal tissue sections were analysed by confocal laser scanning microscopy for the quantification of endostatin-GFP expression. For each group, the value corresponds to the average fluorescence of 5 sections.

Quantitative real-time polymerase chain reaction Five days following the treatment, mice were sacrificed, with eyes being removed and placed in a glass plate containing phosphate buffer saline, the retina was isolated and was kept in liquid nitrogen for -80°C. Retinal samples were used for RNA extraction. Retina tissue of 50 mg was treated with 1 mL TRIzol. The rest of the experimental procedure was the same as the cell experiment.

Western blot analysis Five days after treatment, mice were sacrificed with eyes being harvested and placed in a glass plate containing phosphate buffer saline. The retina was isolated and was kept in liquid nitrogen for -80°C. Cut the retina into pieces and add 1 mL RIPA lysis buffer into 100 mg tissue. Homogenize the tissue and transfer the homogenate to a 1.5 mL centrifuge tube. Centrifuge at 12 000× g, 4°C for 5min (Torikami Kiyo). The supernatant was used for electrophoresis, Western blotting immune precipitation operation. The rest of the experimental procedure was the same as the cell experiment.

Statistical Analysis All data were expressed in the form of mean±standard deviation. SPSS 17.0 software (SPSS Inc., Chicago, IL, USA) assisted in the analysis. $P<0.05$ exhibited statistical significance. The one-way ANOVA assisted in comparing groups. The *t*-test as well as the least significant difference could assist in the further comparisons.

RESULTS

Quantitative Assessment of Gene Transfection in HREC Cultures A laser confocal microscope assisted in observing the GFP expression 24h after transfection (Figure 1A). Numerous cells incubated with CMBs expressed GFP, while few cells incubated with NMBs and liposomes expressed GFP, and the controls with no GFP expression (Figure 1A). The transfection efficiency was determined by the quantification of gene expression. The flow cytometry observed positive GFP expression at 24h and 48h post-transfection. Measurement of the transfection efficiency was completed as the percentage of cells expressing GFP in the population (Figure 1B). The transfection efficiencies regarding the control, NMB, liposome and CMB groups were 1.20%±0.21%, 28.25%±0.57%, 30.74%±7.50% and 41.84%±8.90%, respectively (Figure 1B). The CMB group exhibited a remarkably higher transfection efficiency compared with other groups ($P<0.05$ against the NMB and liposome groups; Figure 1C). Nevertheless, differences between the transfections with the various types of microbubbles after 24h and 48h were not significant ($P>0.05$).

Effect of Gene Transfection on the Cell Cycle For the investigation of the mechanism underlying the observed anti-angiogenesis activity, we conducted cell cycle analyses for identifying the fate of the cells following endostatin-GFP gene transfection. Both flow cytometry and cell cycle analysis were conducted. In repeated experiments, endostatin was shown to inhibit cell cycle progression in endothelial cells in G1 phase (Figure 2A). The cell cycle of HRECs in the CMB group underwent a clear arrest in G1 phase 24h and 48h post-transfection (Figure 2B**)**. Additionally, the percentage of cells remaining in G1 phase increased over time, which could also be found in the control group due to contact inhibition, despite the higher percentage of cells arrested in G1 phase in the CMB group than the other groups ($P<0.05$ against NMBs and liposomes, $P<0.01$ against the control group; Figure 2B). The number of cells in S phase of the cell cycle started to reduce in the CMB group at 24h post-transfection, while that in the other groups did not show a decreasing trend; the cell cycle change trend corresponded to the changes in the percentages of cells in G1 (Figure 2C).

Analysis of the Effect of the Endostatin-GFP Gene on Angiogenesis and HREC Migration We performed a vascular formation experiment following gene transfer to evaluate the angiogenesis effect (Figure 3A). The vascular formation observed *via* microscopy underwent clear inhibition in the CMB groups. Additionally, the vascular tube cavities formed by the HRECs exhibited an obvious decrease relative to the other groups ($P<0.05$ against the NMB group and liposome group, $P<0.01$ against the control groups; Figure 3B). In the NMB and liposome groups, vascular tube cavities formed by HRECs also presented a decrease relative to the control groups ($P<0.05$; Figure 3B); but the two groups did not present significant difference ($P>0.05$; Figure 3B). Hence, there was an obvious increase in the level of endostatin protein following endostatin-GFP gene transfer with CMBs under the mediation of ultrasound, and the increasing levels of endostatin protein were capable of hindering angiogenesis *in vitro*. The CMBs had a higher antiangiogenesis effect than the other groups ($P<0.05$ against the NMB group and liposome group, $P<0.01$ against the control groups).

The number of migrating HRECs decreased concomitant with the inhibition of angiogenesis (Figure 3C and 3D). This result indicates that the enhancement of endostatin protein levels successfully inhibited HRECs migration *in vitro*. Hence, ultrasound-mediated endostatin gene transfer with CMBs can efficiently inhibit angiogenesis and HREC migration.

Histological Results For verifying how endostatin transfection affected retinal neovascularization, we examined the development of endothelial nuclei in new vessels that extended from the retina to the vitreous (Figure 4A). The number of endothelial nuclei in new vessels was significantly lower in the right eye of the mice in the CMB groups than that in the other groups ($P<0.05$ against the NMB group and liposome group, $P<0.01$ against the control groups; Figure 4B). The number of endothelial nuclei representing new vessels was also decreased in the NMB and liposome groups compared with the control

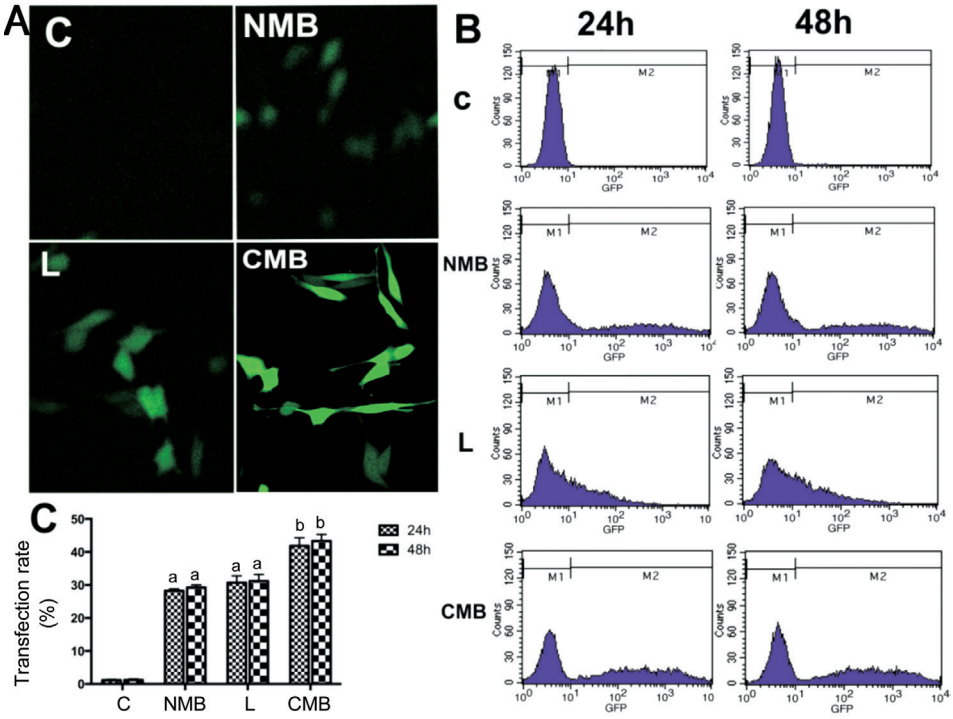

Figure 1 Ultrasound-mediated gene delivery-mediated endostatin-GFP gene transfection in cell culture A: Expression of GFP in HRECs under a laser confocal microscope at 24h post-transfection (20× objective); B: Representative images regarding flow cytometry for quantitative analysis on the transfection efficiency at 24h and 48h post-transfection. The percentages of GFP-positive cells stood for the gene transfection efficiency. C: Statistical analysis on the gene transfection efficiency. CMBs exhibited a higher transfection efficiency after 24h relative to NMBs. (^aP<0.05 against the control and CMB groups; n=6 per group). The difference between 24h and 48h in each group did not present a statistical significance (^bP>0.05). C: Blanked control group; NMB: Endostatin-GFP plasmid under the treatment of NMBs and ultrasound; L: Endostatin-GFP plasmid under the treatment of liposomes; CMB: Endostatin-GFP plasmid under the treatment of CMBs and ultrasound; GFP: Green fluorescent protein; HREC: Human retinal endothelial cells.

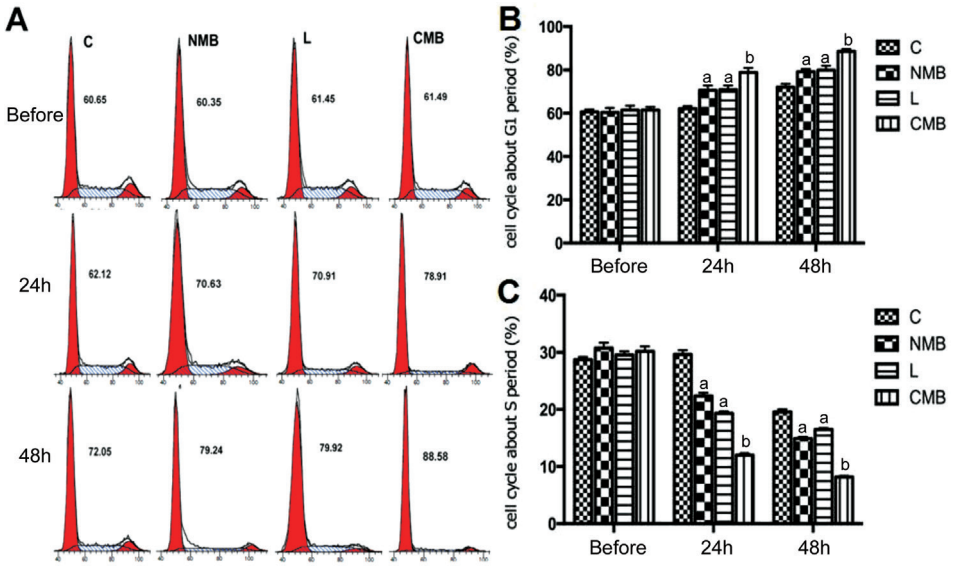

Figure 2 The inhibition of cell cycle within G1 phase is induced by the ransfection of endostatin gene A: DNA content flow cytometric profiles following transfection with the endostatin gene *via* ultrasound with NMBs and CMBs; B: Statistical analysis on the cell cycle in G1 phase. The cell cycle underwent a clear arrest in G1 phase in the CMB groups at 24h and 48h post-transfection. Meanwhile comparisons among the groups were performed. C: Statistical analysis of the cell cycle in S phase. The percentages of HRECs in S phase showed an obvious decrease in the CMB groups at 24h and 48h post-transfection. ^aP<0.05 for the control and CMB groups, ^bP<0.01 for the control; n=6 per group. C: Blanked control group; NMB: Endostatin-GFP plasmid under the treatment of NMBs and ultrasound; L: Endostatin-GFP plasmid under the treatment of liposomes; CMB: Endostatin-GFP plasmid under the treatment of CMBs and ultrasound.

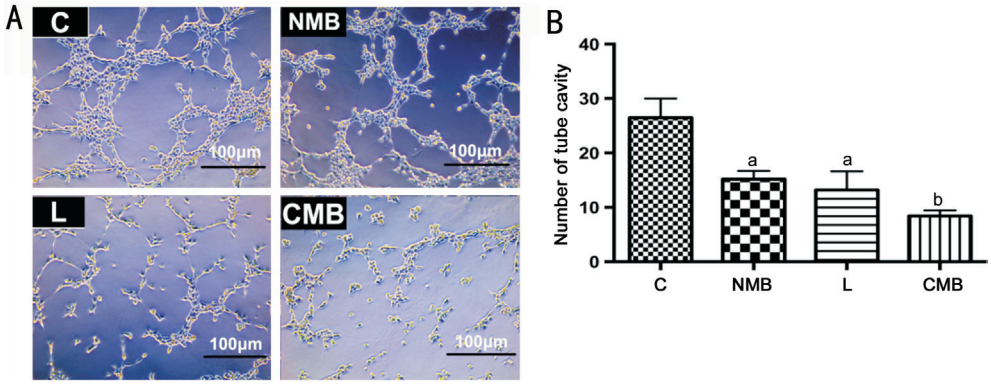

Figure 3 Analysis of how endostatin gene transfer affects *in vitro* angiogenesis and HREC migration A: Vascular tube formation image *in vitro* following ultrasound-mediated endostatin gene transfer with NMBs, liposome and CMBs (10× objective); B: The CMB groups showed clear inhibition of vascular formation *via* direct counting. [a]*P*<0.05 against the control group and CMB group, [b]*P*<0.01 against the control group; *n*=6 per group. C: Blanked control group; NMB: Endostatin-GFP plasmid under the treatment of NMBs and ultrasound; L: Endostatin-GFP plasmid under the treatment of liposomes; CMB: Endostatin-GFP plasmid under the treatment of CMBs and ultrasound; HREC: Human retinal endothelial cells.

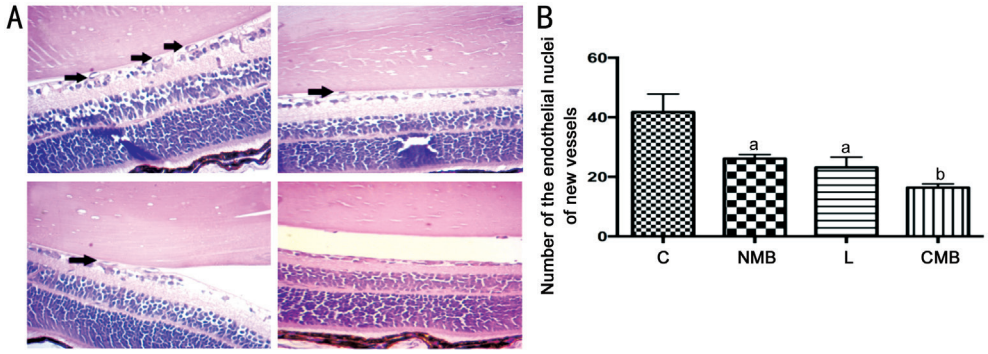

Figure 4 Evaluation of the effect of endostatin on the development of retinal neovascularization A: The number of endothelial nuclei representing new vessels following ultrasound-mediated endostatin gene transfer *in vivo* with NMBs, liposomes and CMBs; B: Direct counting assisted in finding the clear decrease in the endothelial nuclei of the new vessels in the CMB group. [a]*P*<0.05 against the control group and CMB group, [b]*P*<0.01 against the control groups; *n*=6 per group. C: Blanked control group; NMB: Endostatin-GFP plasmid under the treatment of NMBs and ultrasound; L: Endostatin-GFP plasmid under the treatment of liposomes; CMB: Endostatin-GFP plasmid under the treatment of CMBs and ultrasound.

groups, and this difference showed statistical significance (*P*<0.05; Figure 4B); nevertheless, these two groups did not show statistical significance (*P*>0.05; Figure 4B). Hence, ultrasound-mediated endostatin-GFP gene transfer with CMBs was capable of successfully hindering retinal neovascularization *in vivo*. There was a greater antiangiogenesis effect for CMB than the other groups.

Laser Scanning Confocal Microscopy Laser scanning confocal microscope was observed in NMB group, liposome group and CMB group at 5, 14 and 28d after transfection. The expression of endostatin-GFP was observed in all layers of the retina, which was most obvious in the retinal pigment epithelial layer (RPE). Each measuring 5 slices of RPE layer of fluorescent intensity were averaged as fluorescence intensity values (Table 1). The statistical results showed that after transfection at 5 and 14d, the expression intensity of endostatin-GFP in NMB group, liposome group and CMB group were

Table 1 The fluorescent density of pEZ-M46-ES in different groups

Groups	5d	14d	28d
NMB	58.8875±5.5849	133.5363±11.729	128.1250±11.359[b]
L	52.9100±3.7787	138.7350±10.549	105.1350±6.6426
CMB	73.0475±3.3379[a]	193.5363±11.739[a]	181.1250±11.459[a]

[a]*P*<0.05 related to the liposome as well as NMB groups at the same time point, [b]*P*<0.05 related to the liposome groups at the same time point. NMB: Endostatin-GFP plasmid by ultrasound and NMBs; L: Endostatin-GFP plasmids treated by liposomes; CMB: Endostatin-GFP plasmids by ultrasound and CMBs.

all increased gradually (Figure 5), but the expression intensity of endostatin-GFP in 28d group was weaker than that in 14d group, the difference did not show statistical significance (Figure 5); compared with group NMB and liposome group, CMB group presents statistical significance (*P*<0.05). Fluorescence intensity of expression between NMB group and

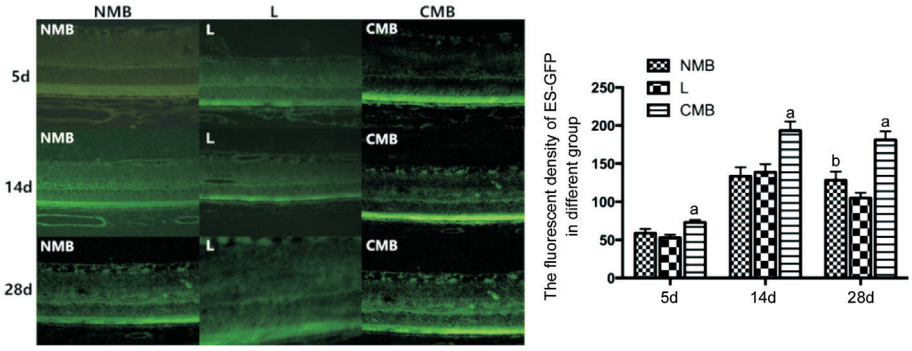

Figure 5 The endostatin-GFP fluorescence expression intensity of NMB, liposome and CMB group at 5, 14, and 28d after transfection Fluorescence intensity of expression between NMB group and liposome group had no significant difference at 5d and 14d after transfection, but the expression intensity of endostatin-GFP in NMB group was stronger than that of liposome group at 28d after transfection. [a]P<0.05 against the NMB and L groups at the same time point, [b]P<0.01 against the L group at the same time point; n=6 per group. C: Blanked control group; NMB: Endostatin-GFP plasmid under the treatment of NMBs and ultrasound; L: Endostatin-GFP plasmid under the treatment of liposomes; CMB: Endostatin-GFP plasmid under the treatment of CMBs and ultrasound.

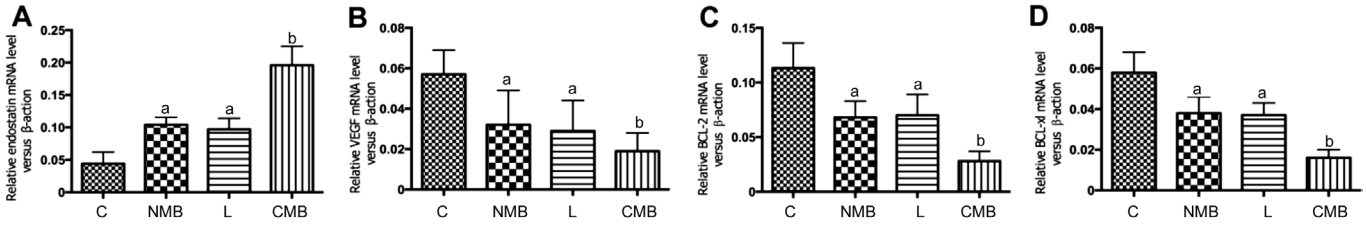

Figure 6 qPCR analysis of the endostatin-GFP plasmid transcription and impact on VEGF, Bcl-2 and Bcl-xl in the retina of mice The endostatin (A) mRNA presented obviously higher levels in the CMB group relative to the other three groups. VEGF (B), Bcl-2 (C) and Bcl-xl (D) mRNA presented obviously lower levels in the CMB group relative to the other three groups. [a]P<0.05 against the control and CMB groups, [b]P<0.01 against the control; n=6 per group. C: Blanked control group; NMB: Endostatin-GFP plasmid under the treatment of NMBs and ultrasound; L: Endostatin-GFP plasmid under the treatment of liposomes; CMB: Endostatin-GFP plasmid under the treatment of CMBs and ultrasound.

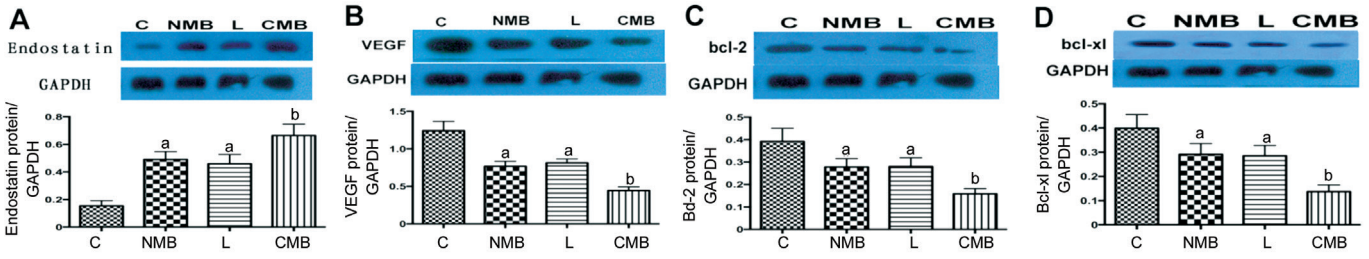

Figure 7 Western blot analyses of the expression of the endostatin protein and the effect on VEGF expression in the retina of mice Endostatin (A) protein levels were significantly higher following CMB delivery of the ES gene compared with the NMB, liposome and control groups. VEGF (B), Bcl-2 (C) and Bcl-xl (D) protein levels were significantly lower following CMB delivery of the ES gene compared with the NMB, liposome and control groups. [a]P<0.05 against the control group and CMB group, [b]P<0.01 against the control group; n=6 per group. C: Blanked control group; NMB: Endostatin-GFP plasmid under the treatment of NMBs and ultrasound; L: Endostatin-GFP plasmid under the treatment of liposomes; CMB: Endostatin-GFP plasmid under the treatment of CMBs and ultrasound.

liposome group had no significant difference at 5 and 14d after transfection, but the expression intensity of endostatin-GFP in NMB group was stronger than that of liposome group at 28d after transfection, and the difference did not show statistical significance (P<0.05).

qPCR Analysis *in vivo* After transfection, the CMB group exhibited the highest endostatin gene transcription level (P<0.05 against the NMB group and liposome group, P<0.01 against the control groups, but the NMB and liposome groups nearly presented no difference (P>0.05). The increase in endostatin mRNA was coupled with the decrease in VEGF, Bcl-2 and Bcl-xlmRNA (Figure 6). This result met the results of *in vitro* experiments.

Western Blotting Analysis *in vivo* After transfection, endostatin protein expression of different groups was shown in the Figure 7, CMB group of protein level was significantly higher than that of the other groups (P<0.05 against the NMB and liposome groups, P<0.01 against the control groups).

NMB groups and liposome groups exhibited increasing endostatin protein levels relative to the control group, and the difference is statistically significant (P<0.05). Corresponding with the CMB group of VEGF, Bcl-2 and Bcl XL protein levels than the other groups decreased significantly (P<0.05 against the NMB and liposome groups, P<0.01 against the control groups), NMB group and L group expressed lower VEGF, Bcl-2 and Bcl XL protein level than the control group, and the difference is statistically significant (P<0.05), but the difference between the two groups was of no statistical differences, and group C see strong protein bands (Figure 7B-7D). The result also met the results of *in vitro* experiments.

Once again, it was proved that ultrasonically irradiated CMBs could improve the expression of endostatin gene in mice retina from the protein level, and increased expression of endostatin can effectively inhibit the VEGF, Bcl-2 and Bcl-xl expression.

DISCUSSION

Retinal neovascularization mainly leads to vision impairment around the world. The regulation of angiogenesis is conducted by balancing the angiogenic regulators and angiostatic regulators, which operates continuously including vascular endothelial cell activation, migration, and proliferation. Endostatin has been identified as an effective antiangiogenesis agent, which especially restrains the proliferation and migration of vascular endothelial cell. The endostatin seemly exhibits a more obvious effect relative to the effect that could be observed after the incubation with VEGF antibodies. Previous reports have demonstrated that endostatin treatment has the following effects: 1) activating caspase-3 and lowering the Bcl-2 to Bax ratio, resulting in the induction of apoptosis[20]; 2) inducing tyrosine kinase activity and enhancing apoptosis in fibroblast growth factor (FGF)-treated endothelial cells, thereby reducing the proportion of cells in S phase and contributing to the stagnation of endothelial cells in G1 phase[21]; 3) directly interacting with the VEGF receptor KDR/Flk 1, thereby blocking VEGF-mediated signal transduction[22]; 4) modulating cellular functions such as migration and survival in an integrin-dependent manner[23]; 5) interacting with tropomyosin, which disrupts the integrity of microfilaments, inhibits cell motility and induces apoptosis[24]; and 6) inhibiting VEGF mRNA gene expression, resulting in inhibition of the formation of retinal neovascularization[25].

The ultrasound-mediated gene delivery is with great promise to be a noninvasive and non-viral gene therapy strategy and has been widely researched since it first appeared[26-27]. The gene transfection efficiency depends on multiple factors, like the acoustic intensity, pulse sequence, and DNA concentration [28-31].

An interesting phenomenon associated with ultrasound-mediated gene delivery is that the resultant cell viability shows a reverse relation to the transfection efficiency. Specifically, with increasing microbubbles concentrations, the transfection efficiency increases, while the cell viability decreases. Previous research indicated the relationship between transfection efficiency and acoustic intensity was nonlinear. Whereas, it is necessary to adjust the acoustic intensity at site, pulsing sequence, and microbubble concentration for getting optimal conditions, taking in to account the tradeoff between cell viability and the transfection efficiency. Our early experiment presented that majorities of cells could survive under certain conditions: 1 W/cm^2 sound intensity, 1min irradiation time, 20% duty cycle and 10% microbubble concentration. On that account, the research adopted above optimal conditions.

Obviously, the usage of CMBs helped to achieve a significantly greater DNA-binding capacity[32-34]. Similarly, we observed the CMB group exhibited greater the fluorescence intensity relative to the other groups under the laser confocal microscope. Based on flow cytometry, the transfection efficiencies obtained for the endostatin-GFP plasmid using NMBs, liposomes and CMBs at 24h post-transfection were 28.25%±0.57%, 30.74%±7.50% and 41.84%±8.90%, respectively. These results revealed the successful transfection of endostatin-GFP gene into the target cells using the ultrasound-mediated gene delivery method. We also analyzed the therapeutic effect exerted by endostatin on the cell cycle, angiogenesis *in vitro*, HREC migration and the formation of retinal neovascularization *in vivo*. All these proved the better treatment effect by using CMBs relative to NMBs or liposomes. ES gene therapy that employed ultrasound-mediated gene delivery seems to be a proper antiangiogenesis therapy methodology relying on its capability of overcoming the endostatin-related instability defect.

Besides, we found the fluorescence intensity of endostatin-GFP was not significantly different between NMB and liposome group at 5 and 14d after transfection, but it was higher in NMB group than that in liposome group at 28d. In the early gene transfection stage, ultrasound-mediated gene delivery and liposome exhibited no significant difference, however, in the long-term ultrasound-mediated gene delivery revealed more expression of target gene. This phenomenon may be because ultrasound-mediated gene delivery of cells or tissues is mainly affected by the “sound hole effect” and “cavitation”, while liposome mediated gene transfection depends critically on electrostatic adsorption. For ultrasound-mediated gene delivery, ultrasonic energy and microbubbles rupture may be produced by shock wave, and the shock wave to the intracellular transport can promote the DNA escape from endocytosis bubbles into the nucleus, which makes endogenous genes to be more firmly combined with the expression stability.

There are some limitations in our research. The potential toxicity largely caused by the high CMB and DNA doses prevents cationic lipids from being applied to gene therapy

in vitro and *in vivo*. Further studies addressing the safety of CMBs are still needed. Moreover, it is still needed to further investigate the association among the three indicators of CMBs, namely the zeta potential, the plasmid loading capacity and the transfection efficiency

In conclusion, ultrasound-mediated gene delivery using CMBs is capable of effectively delivering an endostatin-GFP plasmid to HRECs as well as inhibiting retinal neovascularization in mice. The transfection efficiency of the CMBs expressed a significant increase in the transfection efficiency relative to NMBs and liposomes. With increasing transfection efficiency, endostatin exhibited an increasing expression after being treated with CMBs *in vitro* and *in vivo*, and VEGF, Bcl-2 and Bcl-xl exhibited a decreasing expression. Based on above data, CMBs can better enhance ultrasound-mediated gene delivery (UMGD) both *in vitro* and *in vivo*. CMBs can be potentially used for gene therapy as an effective ultrasound contrast agent.

ACKNOWLEDGEMENTS

Authors' contributions: Wu MX and Xu Y performed the experiment; Zhou Y and Zhou XY took charge of data analysis; Wu MX took charge of writing the manuscript; The final manuscript has been read and approved by all authors.

Foundation: Supported by the National Natural Science Foundation for Youth of China (No.81901765).

Conflicts of Interest: Wu MX, None; **Zhou Y,** None; **Zhou XY,** None; **Xu Y,** None.

REFERENCES

1 Casini G, Dal Monte M, Fornaciari I, Filippi L, Bagnoli P. The β-adrenergic system as a possible new target for pharmacologic treatment of neovascular retinal diseases. *Prog Retin Eye Res* 2014;42:103-129.

2 O'Reilly MS, Boehm T, Shing Y, Fukai N, Vasios G, Lane WS, Flynn E, Birkhead JR, Olsen BR, Folkman J. Endostatin: an endogenous inhibitor of angiogenesis and tumor growth. *Cell* 1997;88(2):277-285.

3 Behl T, Kotwani A. Possible role of endostatin in the antiangiogenic therapy of diabetic retinopathy. *Life Sci* 2015;135:131-137.

4 Matsumoto G, Hirohata R, Hayashi K, Sugimoto Y, Kotani E, Shimabukuro J, Hirano T, Nakajima Y, Kawamata S, Mori H. Control of angiogenesis by VEGF and endostatin-encapsulated protein microcrystals and inhibition of tumor angiogenesis. *Biomaterials* 2014;35(4):1326-1333.

5 Taniyama Y, Azuma J, Kunugiza Y, Iekushi K, Rakugi H, Morishita R. Therapeutic option of plasmid-DNA based gene transfer. *Curr Top Med Chem* 2012;12(15):1630-1637.

6 Li HL, Qian J, Yao CF, Wan CF, Li FH. Combined ultrasound-targeted microbubble destruction and polyethylenimine-mediated plasmid DNA delivery to the rat retina: enhanced efficiency and accelerated expression. *J Gene Med* 2016;18(4-6):47-56.

7 Miller DL, Pislaru SV, Greenleaf JE. Sonoporation: mechanical DNA delivery by ultrasonic cavitation. *Somat Cell Mol Genet* 2002;27(1-6): 115-134.

8 Qin P, Han T, Yu ACH, Xu L. Mechanistic understanding the bioeffects of ultrasound-driven microbubbles to enhance macromolecule delivery. *J Control Release* 2018;272:169-181.

9 Burgess MT, Porter TM. Control of acoustic cavitation for efficient sonoporation with phase-shift nanoemulsions. *Ultrasound Med Biol* 2019;45(3):846-858.

10 Manta S, Renault G, Delalande A, Couture O, Lagoutte I, Seguin J, Lager F, Houzé P, Midoux P, Bessodes M, Scherman D, Bureau MF, Marie C, Pichon C, Mignet N. Cationic microbubbles and antibiotic-free miniplasmid for sustained ultrasound-mediated transgene expression in liver. *J Control Release* 2017;262:170-181.

11 Christiansen JP, French BA, Klibanov AL, Kaul S, Lindner JR. Targeted tissue transfection with ultrasound destruction of plasmid-bearing cationic microbubbles. *Ultrasound Med Biol* 2003;29(12):1759-1767.

12 Haag P, Frauscher F, Gradl J, Seitz A, Schäfer G, Lindner JR, Klibanov AL, Bartsch G, Klocker H, Eder IE. Microbubble-enhanced ultrasound to deliver an antisense oligodeoxynucleotide targeting the human androgen receptor into prostate tumours. *J Steroid Biochem Mol Biol* 2006;102(1-5):103-113.

13 Carson AR, McTiernan CF, Lavery L, Hodnick A, Grata M, Leng XP, Wang JJ, Chen XC, Modzelewski RA, Villanueva FS. Gene therapy of carcinoma using ultrasound-targeted microbubble destruction. *Ultrasound Med Biol* 2011;37(3):393-402.

14 Tlaxca JL, Anderson CR, Klibanov AL, Lowrey B, Hossack JA, Alexander JS, Lawrence MB, Rychak JJ. Analysis of *in vitro* transfection by sonoporation using cationic and neutral microbubbles. *Ultrasound Med Biol* 2010;36(11):1907-1918.

15 Nomikou N, Tiwari P, Trehan T, Gulati K, McHale AP. Studies on neutral, cationic and biotinylated cationic microbubbles in enhancing ultrasound-mediated gene delivery *in vitro* and *in vivo*. *Acta Biomater* 2012;8(3):1273-1280.

16 Wang DS, Panje C, Pysz MA, Paulmurugan R, Rosenberg J, Gambhir SS, Schneider M, Willmann JK. Cationic versus neutral microbubbles for ultrasound-mediated gene delivery in cancer. *Radiology* 2012;264(3):721-732.

17 Sun L, Huang CW, Wu J, Chen KJ, Li SH, Weisel RD, Rakowski H, Sung HW, Li RK. The use of cationic microbubbles to improve ultrasound-targeted gene delivery to the ischemic myocardium. *Biomaterials* 2013;34(8):2107-2116.

18 Panje CM, Wang DS, Pysz MA, Paulmurugan R, Ren Y, Tranquart F, Tian L, Willmann JK. Ultrasound-mediated gene delivery with cationic versus neutral microbubbles: effect of DNA and microbubble dose on *in vivo* transfection efficiency. *Theranostics* 2012;2(11):1078-1091.

19 Xu Y, Xie ZY, Zhou Y, Zhou XY, Li P, Wang ZG, Zhang QX. Experimental endostatin-*GFP* gene transfection into human retinal vascular endothelial cells using ultrasound-targeted cationic microbubble destruction. *Mol Vis* 2015;21:930-938.

20 Ling Y, Lu N, Gao Y, Chen Y, Wang S, Yang Y, Guo QL. Endostar induces apoptotic effects in HUVECs through activation of caspase-3 and decrease of Bcl-2. *Anticancer Res* 2009;29(1):411-417.

21 Dixelius J, Larsson H, Sasaki T, Holmqvist K, Lu L, Engström A, Timpl R, Welsh M, Claesson-Welsh L. Endostatin-induced tyrosine kinase signaling through the Shb adaptor protein regulates endothelial cell apoptosis. *Blood* 2000;95(11):3403-3411.

22 Klinnikova MG, Bakarev MA, Nikityuk DB, Lushnikova EL. Immunohistochemical study of the expression of vascular endothelial growth factor receptor-2 (KDR/flk-1) during myocardial infarction. *Bull Exp Biol Med* 2017;163(4):500-505.

23 Rehn M, Veikkola T, Kukk-Valdre E, Nakamura H, Ilmonen M, Lombardo CR, Pihlajaniemi T, Alitalo K, Vuori K. Interaction of endostatin with integrins implicated in angiogenesis. *Proc Natl Acad Sci U S A* 2001;98(3):1024-1029.

24 MacDonald NJ, Shivers WY, Narum DL, Plum SM, Wingard JN, Fuhrmann SR, Liang H, Holland-Linn J, Chen DH, Sim BK. Endostatin binds tropomyosin. A potential modulator of the antitumor activity of endostatin. *J Biol Chem* 2001;276(27):25190-25196.

25 Jo DH, Kim S, Kim D, Kim JH, Jon S, Kim JH. VEGF-binding aptides and the inhibition of choroidal and retinal neovascularization. *Biomaterials* 2014;35(9):3052-3059.

26 Tran DM, Zhang F, Morrison KP, Loeb KR, Harrang J, Kajimoto M, Chavez F, Wu L, Miao CH. Transcutaneous ultrasound-mediated nonviral gene delivery to the liver in a porcine model. *Mol Ther Methods Clin Dev* 2019;14:275-284.

27 Chen HH, Matkar PN, Afrasiabi K, Kuliszewski MA, Leong-Poi H. Prospect of ultrasound-mediated gene delivery in cardiovascular applications. *Expert Opin Biol Ther* 2016;16(6):815-826.

28 Karshafian R, Bevan PD, Williams R, Samac S, Burns PN. Sonoporation by ultrasound-activated microbubble contrast agents: effect of acoustic exposure parameters on cell membrane permeability and cell viability. *Ultrasound Med Biol* 2009;35(5):847-860.

29 Noble-Vranish ML, Song SX, Morrison KP, Tran DM, Sun RR, Loeb KR, Keilman GW, Miao CH. Ultrasound-mediated gene therapy in swine livers using single-element, multi-lensed, high-intensity ultrasound transducers. *Mol Ther Methods Clin Dev* 2018;10:179-188.

30 Zarnitsyn VG, Prausnitz MR. Physical parameters influencing optimization of ultrasound-mediated DNA transfection. *Ultrasound Med Biol* 2004;30(4):527-538.

31 Tran DM, Harrang J, Song SX, Chen J, Smith BM, Miao CH. Prolonging pulse duration in ultrasound-mediated gene delivery lowers acoustic pressure threshold for efficient gene transfer to cells and small animals. *J Control Release* 2018;279:345-354.

32 Delalande A, Bastié C, Pigeon L, Manta S, Lebertre M, Mignet N, Midoux P, Pichon C. Cationic gas-filled microbubbles for ultrasound-based nucleic acids delivery. *Biosci Rep* 2017;37(6):BSR20160619.

33 Zhou Y, Gu HT, Xu Y, Li F, Kuang SJ, Wang ZG, Zhou XY, Ma HF, Li P, Zheng YY, Ran HT, Jian J, Zhao YJ, Song WX, Wang QS, Wang D. Targeted antiangiogenesis gene therapy using targeted cationic microbubbles conjugated with *CD105* antibody compared with untargeted cationic and neutral microbubbles. *Theranostics* 2015;5(4):399-417.

34 Liu YY, Zhou YL, Xu JF, Luo H, Zhu Y, Zeng XX, Dong FJ, Wei ZH, Yan F, Zheng HR. Ultrasound molecular imaging-guided tumor gene therapy through dual-targeted cationic microbubbles. *Biomater Sci* 2021;9(7):2454-2466.